Proceedings of IMECE'03
2003 ASME International Mechanical Engineering Congress & Exposition
Washington, D.C., November 16-21, 2003

IMECE2003-42082

DESIGN OF A MICROFABRICATED RANKINE CYCLE STEAM TURBINE FOR POWER GENERATION

Luc G. Fréchette*, Changgu Lee, Selin Arslan, and Yuan-Chun Liu
Columbia University
Department of Mechanical Engineering
500 West 120th Street, New York NY, 10027

ABSTRACT

This paper presents the system-level and component design of a micro steam turbine power plant-on-a-chip which implements the Rankine cycle for micro power generation. The microfabricated device consists of a steam turbine that drives an integrated micropump and generator. Two-phase flow heat exchangers are also integrated on-chip with the rotating components to form a complete micro heat engine unit, converting heat to electricity. The system-level design includes cycle analysis and overall performance predictions, accounting for the expected performance of miniaturized components, thermal and structural integrity of the microsystem, and system-level trade-offs for optimal overall performance. Operating principles and design studies are also presented for the core component, with emphasis on a multistage, planar, radial microturbine and a spiral groove viscous pump. Design consideration for two-phase flow heat exchangers, microbearings, seals and micro-generators are also presented. Expected power levels range from 1-12 W per chip with energy conversion efficiency in the range of 1-11%. This suggests power density of up to 12 kW/kg for this technology, which is an order of magnitude greater than competing technologies, such as thermoelectrics. This study suggests the viability of a micro Rankine power plant-on-a-chip, but also identifies critical engineering challenges that must be met for practical implementation.

Keywords: MEMS, micro power generation, microturbine, micropump.

INTRODUCTION

The advent of microelectromechanical systems (MEMS) technology has opened the door to the creation of power systems at unprecedented small scales. Using silicon microfabrication processes, it has been suggested that common power generation systems could be miniaturized yielding high-power density, low-cost, batch manufactured power sources, or *Power MEMS* [1]. Such power sources would provide alternatives to today's batteries, with potentially higher energy densities since they could extract energy from hydrocarbon fuels.

Since the mid-1990's, development efforts have been initiated to create MEMS-based heat engines, such as gas turbine engines ([2]-[4]), internal combustion engines (rotary Wankel [5] or piston [6]), and thermal-expansion-actuated piezoelectric power generators ([7],[8]). These microengines convert thermal energy (from combustion of a fuel or another heat source), sequentially into fluid, mechanical, then electrical energy. In addition, various static approaches to directly convert heat into electricity are in development for small scale applications, including thermoelectric ([9],[10]), thermionic [11], and thermophotovoltaic [12] components coupled with a heat source. The engineering challenges to develop such multifaceted and integrated microsystems remain significant; hence most achievements to date have been for subsystems and typically at low performance levels. Further research efforts are therefore warranted to assess the viability and performance of these and other approach for portable power generation.

The concept developed herein consists of a microfabricated steam turbine power plant-on-a-chip, delivering electricity by scavenging waste heat or through combustion of a fuel. The fabrication approach is based on lithography, deep reactive ion etching, and aligned bonding of silicon and glass wafers. This micro heat engine implements a closed Rankine power cycle using a high speed microturbine with an integrated pump and generator, as well as on-chip heat exchangers. As illustrated in Figure 1, a working fluid in liquid phase is compressed with a pump (states 3 to 4) and then evaporated (state 1') and superheated to a maximum cycle temperature (state 1, T_{max}) through one of the on-chip heat exchangers. The working fluid in vapor form then expands through a turbine (state 1 to 2) to provide mechanical shaft power to drive the pump and an integrated micro-generator. The cycle is closed by condensing the working fluid (state 3 to 4) by rejecting heat to the surroundings. Each power plant chip is expected to generate in the range of 1-10 Watts of electrical power and is nominally 3 mm thick by 1 cm^2 (planar form). A heat supply, heat sink, and power electronics are also required in order to form a complete power generation system.

A single micro Rankine device coupled with a fuel burner could be used as a compact power generator for portable electronics, distributed sensors, and other small scale applications. These micro heat engines could also be useful to

* Corresponding author - phone: (212) 854-2962; e-mail: lucf@alum.mit.edu

generate power from solar radiation or scavenge energy from waste heat, acting for example as a bottoming cycle for other heat engines by covering the engine and exhaust with an array of such chips; the output power then scales proportionally with covered area. Since operating conditions can vary widely depending on the actual application, this initial development effort focused on two applications with significantly different ambient temperatures:

1) Ground power generation: the device is cooled with room temperature air (T_{amb}=25˚C) and forced convection is required (cooling fan needed);
2) Aircraft in-flight power generation, the device is cooled with ambient air (T_{amb}= -50˚C) and forced cooling is available from motion of the aircraft.

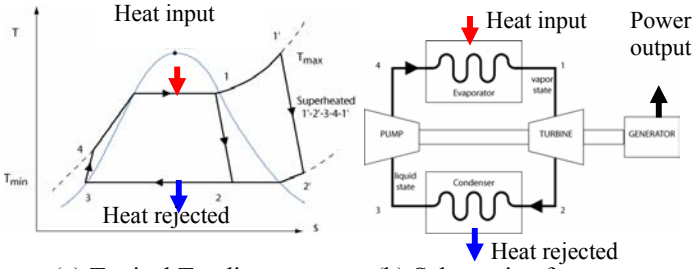

(a) Typical T-s diagram (b) Schematic of system

Figure 1 - Standard superheated Rankine power cycle

This paper presents the preliminary design of a micro Rankine device to assess the feasibility of implementing such a concept through MEMS-based technology. First, the overall device configuration is presented, followed by a cycle analysis to determine the impact of component inefficiencies and define a viable operating space. Preliminary design assessment of the main components is then presented, covering the turbine, pump, generator, heat exchangers, bearings and seals. Predictions of system-level performance for both applications above are then presented. Finally, viability of the approach and the main engineering challenges are discussed.

SYSTEM-LEVEL DESIGN

Device Configuration

The simplified device configuration is shown in Figure 2. It consists of a multi-wafer stack that encloses all the components, including a disk-shaped rotor, microchannels, and electromechanical components. The rotor disk has a planar multistage turbine on one side and a micro-generator on the opposite side. A spiral groove viscous pump is etched at the inner radius of the disk, inboard of the generator, and delivers pressurized liquid through a center hole in the rotor disk. The pressurized working fluid then flows through a microchannel heat exchanger covering the hot side of the chip, to completely evaporate and be superheated. The vapor returns to the center to flow radially outwards along the top side of the rotor disk, through concentric turbine stages, each consisting of a stationary row of blades (attached to the top plate) interdigitated with a rotating blade row that extends from the disk. Vapor flow exiting the turbine proceeds to the second microchannel heat exchanger located on the cold side of the chip to condense before returning to the pump. Seals are required on both sides of the disk to constrain the liquid within the pump and central area. Heat is supplied to the cycle from one outer surface of the chip ("hot side") and removed from the opposite surface ("cold side").

Fluid film bearings support the rotor in the radial and axial directions. A hydrostatic journal bearing is located at the outer diameter of the disk, lubricated by the pressurized working fluid in vapor state. A pair of axial thrust bearings is formed by the viscous pump on the back side and a spiral groove on the face of the forward seal. The overall dimensions of the device are less than 3 mm thick x 1 cm^2.

Compared with internal combustion and gas turbine engines, the proposed Rankine device: 1) operates on a closed cycle, with the working fluid chosen to be water; 2) pumps a liquid instead of compressing a gas, which dramatically reduces the compression work and allows higher pressures; 3) adds heat to the working fluid via a heat exchanger as opposed to direct combustion, allowing a wide range of heat sources; 4) must reject heat to the surroundings through a heat exchanger, as opposed to simply rejecting hot gases to the ambient.

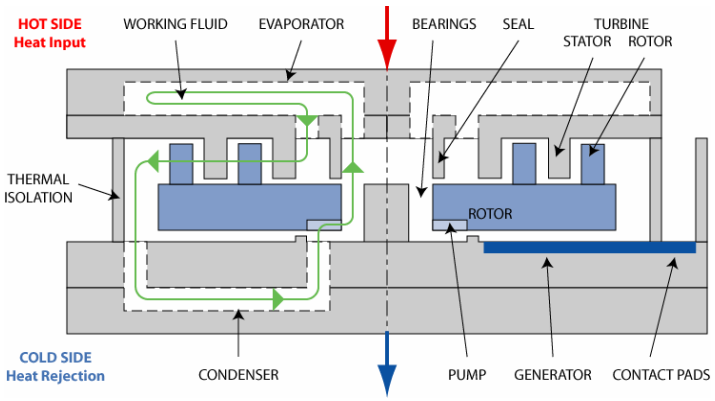

Figure 2 - Cross-section schematic of micro steam-turbine power plant-on-a-chip. Constructed from 5 silicon wafers that are deep reactive ion etched and bonded to integrate the components on a single chip.

Proposed Fabrication Approach

The fabrication approach for the steam turbine power plant-on-a-chip is based on silicon microfabrication technology. First, the electrical components are fabricated on silicon wafers using thin and thick film processing and lithography. Shallow features, such as tip clearance, seal gaps, and grooves for the viscous pumps, are then lithographically defined and etched. Deep structures, such as turbine blades and flow channels, are then formed into the bulk of the silicon wafers by deep reactive ion etching (DRIE) of lithographically-defined features on both sides of the wafers. Through hole are created when deep etched features from both sides of a wafer intersect. The final device is formed by bonding the silicon wafers, creating a laminated, monolithic static structure with integrated quasi-three dimensional flow paths. The single-crystal silicon rotor is enclosed in the static structure and naturally integrated the other components. This approach has been initially developed at MIT for the fabrication of high performance micro-machinery, such as micro gas turbine engines and generators [2]. Single crystal silicon has been demonstrated as a viable material for high-performance micro-machinery, even though geometric design flexibility is limited by the 2D nature of etching. DRIE

and wafer bonded silicon structures have sustained high-speed rotation [13], high temperature gases in micro-combustors [14], and high pressures in micro rocket engines [15]. Furthermore, the integration of a thin film micromotor within a bonded wafer stack has been demonstrated [16].

Although this fabrication approach is appropriate for most of the requirements, such as high speed rotation, high pressure operation, and integration of electromechanical components, it lacks thermal isolation capabilities. Conduction through the structure separating the evaporator from the condenser must be minimized to maintain acceptable efficiency. A central layer formed of low conductivity material, such as glass, is required. The impact of thermal isolation on device performance will be discussed later, after the cycle analysis and presentation of component designs.

Cycle Analysis

Fundamentally, thermodynamics are not a function of scale. Practically however, component efficiencies are typically lower than their large scale brethren and high heat fluxes are required in the heat exchangers. The following sections assess the impact of these practicalities on cycle efficiency and power output, as well as define a baseline cycle. Thermodynamic cycle analysis was performed for both applications in order to evaluate the potential performance of a Rankine cycle. Water is used as the working fluid, and component efficiencies of 5% for the pump and 70% for the turbine are assumed, as discussed in the component design sections later.

A main constrain for such a heat engine is the capability to expel the high heat flux from the condenser, which is on the order to 50-100 W/cm^2. Although in-flight applications could use the air flow around the aircraft for cooling, ground applications would require a fan to provide forced convective cooling. The study considered the trade-off between external cooling power required for the ground application, and the impact of condenser temperature on cycle efficiency. Higher condenser temperature enhanced the heat removal rates, but reduced the Rankine cycle efficiency. Optimum condenser temperatures of 93.5˚C and 10˚C were found for the ground and in-flight applications respectively, in order to maximize the net output electrical power.

Figure 3 shows the cycle efficiency and specific shaft power (power per unit mass flow rate) for both applications, over a range of turbine inlet temperatures (T_{max}) and pump exit pressure (P_{max}). These charts suggest that the efficiency and specific power increase with turbine inlet temperature and pressure, but with limited returns and reduced specific power above 4 MPa. The cycle efficiency and specific power was also found to be essentially linearly dependant on the turbine efficiency, but barely affected by pump efficiency, for turbine inlet pressures below 4 MPa. At higher pressures, the pump power tends to increase faster than the turbine power, due to the low pump efficiency (5%).

For the component design studies presented herein, a nominal mass flow rate of 24 mg/s and a chip size of 1cm^2 were chosen, for external heat transfer considerations in the condenser side. For reference, a temperature-entropy diagram is shown in Figure 4 for a pump exit pressure of 0.5 MPa, superheated temperature T_{max}=400°C, and condenser temperature T_{min}=10°C. It shows that the pump power is on the order of 1% of the turbine power, and that most of the heat addition occurs in the two-phase flow region.

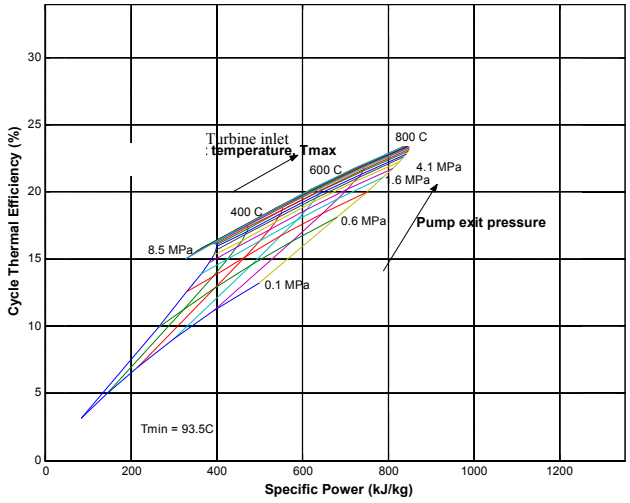

(a) ground-based application (T_{min} = 93.5˚C)

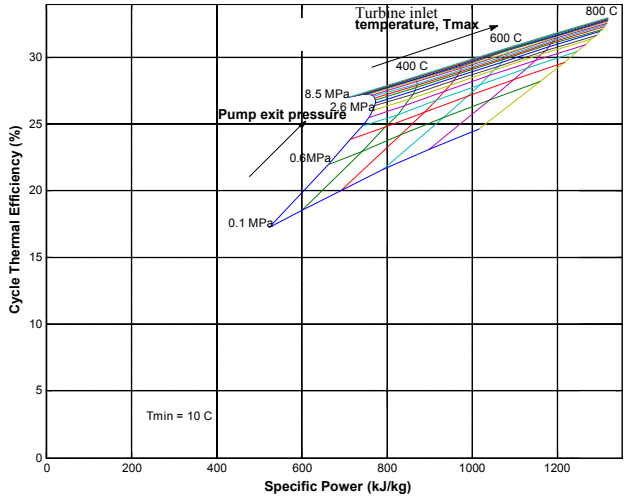

(b) in-flight application (T_{min} = 10˚C)

Figure 3 - Baseline cycle efficiency and specific power as a function of pump exit pressure and superheated turbine inlet temperature (water, assuming η_p=5%, η_t=70%).

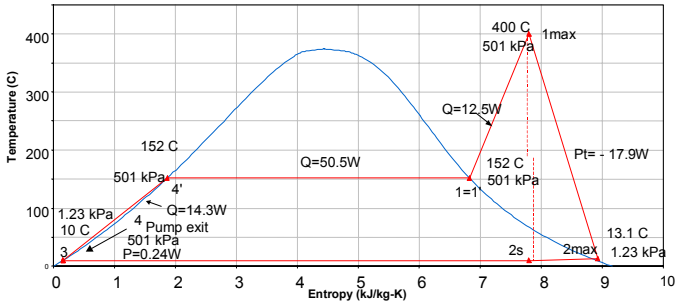

Figure 4 - Temperature-entropy diagram of the Rankine cycle for typical design conditions (water, 24 mg/s, T_{min}=10°C, T_{max}=400°C, P_{max}=0.5 MPa).

COMPONENT DESIGN

Most of the components required for this microsystem have not yet been development at small-scales and for MEMS-based implementation. In this section, the preliminary design of the main components is presented, aiming at defining the viability of the proposed concept and to scope the design space.

Turbine

A key component of the system is the turbine, which converts fluid power to mechanical power to drive the pump, the generator, and counter friction losses on the rotor. As suggested by the cycle studies, high pressure differentials on the order of tens of atmospheres are desirable. In order to stay within a conservative aerodynamic and mechanical design space (200-400 m/s tip speed), a multistage turbine was found to be necessary. Since the turbine blades are formed in a single, common etch step, all blades are constrained to a uniform height, h. Due to this limitation of silicon micromachining and the planar geometry, the design space is significantly different than for traditional turbomachinery. The main differences are that:

1) each stage (blade row) operates at a different tip speed, proportional to the radius: $U = \Omega \cdot r$;
2) the throughflow area increases linearly with radius: $A(r) = 2\pi \cdot r \cdot h$ with constant blade height, h, which imposes area variations across each blade row, and from stage to stage;
3) blade shapes are constrained to 2D extruded-like shapes, without any twist along the span.

A design approach for multi-stage planar turbines was developed based on traditional meanline design methods for turbomachinery [17] (with the particularities of the radial geometry): conservation of rothalpy across a blade row (in the relative frame), relative total pressure drop across the blade row specified by an empirical loss coefficient, and exit relative flow angles specified by the designer. For this preliminary study, flow is considered to be adiabatic, blockage is neglected (actual geometric area is used), and deviation is assumed to be constant over the range of operation. Thermodynamic fluid properties were defined using computerized steam tables. To maintain a conservative aerodynamic design, ensure robustness, and leverage previous experience, the relative exit flow angle was limited to 60° from the radial direction and the maximum tip speed to 300 m/s. This simple modeling was used to calculate the expected power levels as a function of the main design parameters, such as rotor diameter, blade chord, rotational speed, and number of stages, as well as characterize the loading distribution across the stages.

For the baseline mass flow of 24 mg/s, a power level of 1W (40 kJ/kg) per stage was easily achieved with the above constraints. In order to match the specific power levels defined in the cycle analysis, 10 to 30 stages are expected to be required. It is difficult however to match more than 5 stages on a single rotor, since they operate with different tip speeds and flow areas dictated by the change of radius. A single rotor is therefore expected to provide on the order of 5 W of mechanical power (200 kJ/kg). Optimum diameter of a single rotor was found to be on the order of 2 mm.

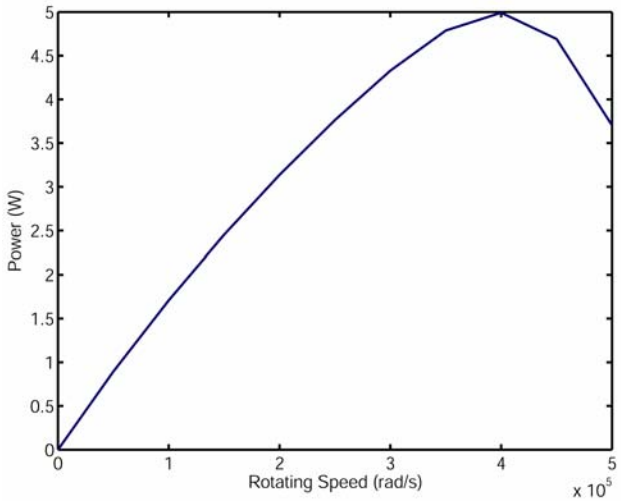

(a) Total Power

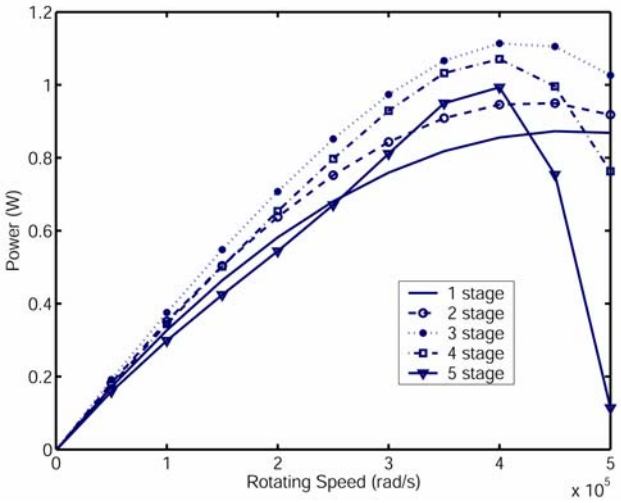

(b) Power from each stage of turbine

Figure 5 - Performance of 5 stage turbine at inlet condition of 400°C, 0.6MPa and steam flow rate of 24 mg/s.

Table 1 – Single-rotor microturbine configuration and operating conditions.

Inlet/Exit Pressure	0.60 to 0.18 MPa
Inlet/Exit Temp.	400°C to 316°C
Inner/Outer Radius	360 to 760 microns
Blade chord	Range: 20 to 50 microns
Flow exit angle (rel.)	60°, except 4th rotor: 55°, 5th rotor: 50°
Mass flow	24 mg/s
Rotational speed	4x10^5 rad/s (tip speed 305 m/s)
Total power	5W

Figure **5** illustrates the power from a single multi-stage rotor as a function of rotational speed, illustrating that it is possible to match the stages to all operate at their optimum conditions at the same speed of 4x10^5 rad/s. The microturbine design and operating conditions are summarized in Table 1. Rotor and stator isentropic efficiencies of 70% are assumed, based on CFD analysis of microturbomachinery [18]. Since the rotor diameter is significantly less than the chip size, multiple spools (rotors) per chip can be used to achieve a broad range of power levels. Preliminary design was also developed for a 28

W (1150 kJ/kg) multiple rotor configuration, which consists of five individual rotors with power levels ranging from 3.8 to 8.4W. It operates with an inlet pressure of 8 MPa and temperature of 780°C. The 5W single-rotor configuration discussed above is similar to the third of the five rotors.

To this point, turbine design investigations have been based on a meanline analysis, assuming turbine efficiency. Four main aspects will require further investigation: 1) effect of scale and 2D geometry on turbine efficiency (blade profile losses); 2) maximum blade loading at low Reynolds numbers, to define design limitations for power levels per stage; 3) effect of non-adiabatic operation and impact on robustness; and 4) three-dimensional and secondary flows, such as tip clearance, hub and shroud boundary layers, and non-uniform inlet flow.

Pump

Two types of pumps were initially considered for the Rankine device: 1) turbomachinery-based pumps, and 2) viscous pumps. Given the very small volumetric flow rate of the working fluid in liquid form (1500 times less than in vapor phase), Reynolds numbers are very low and momentum-based pumping principles, such as turbomachinery, become increasingly less efficient. Furthermore, the very small scale (orders of magnitude smaller than the turbine described above) deem the turbomachinery approach to be impractical from a fabrication standpoint. Given the non-stringent requirement on pump efficiency (as described in the Cycle Analysis section earlier), a spiral groove viscous pump was found to be preferable and was designed for this application.

As illustrated in Figure 6, it consists of a polar array of shallow radial grooves inclined at a constant spiral angle, α, that rotate parallel to a planar surface. The configuration is readily micromachined on the back side of the rotor and integrated with the other Rankine device components. The design is directly inspired from hydrodynamic spiral groove thrust bearings, with a center port added to collect the pressurized fluid. Traditionally, spiral groove thrust bearings and other lubricating flows have been designed and analyzed using the Reynolds equation, which assumes fully developed viscous flow and uniform pressure and density across the thickness of the lubricating film. This approach, with the inclusion of radial flow, is applicable for the microscale viscous pump. The pressure rise, torque and power consumption as a function of geometry, rotational speed and flow rate can be determined based on published work on macroscale spiral groove viscous pumps ([19],[20],[21]).

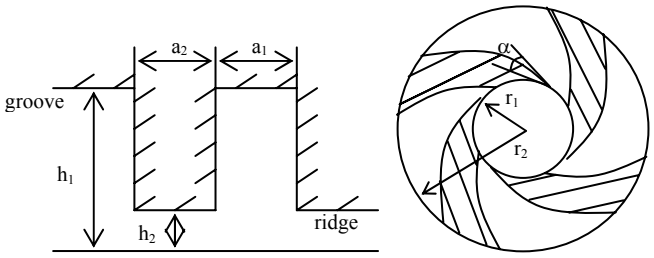

(a) cross-section view (b) plan view

Figure 6 - Spiral groove viscous pump configuration (less grooves are shown for clarity).

Table 2 - Optimized configurations of low pressure and high pressure viscous pumps.

ΔP	0.6MPa	8MPa
Rotational speed	4×10^5 rad/s	4×10^5 rad/s
Spiral angle	15°	15°
Groove depth, h_1	4.6 μm	3.1 μm
Clearance, h_2	0.6 μm	0.5 μm
Inner radius, r_1	214 μm	243 μm
Outer radius, r_2	275 μm	450 μm
Power consumption	0.35 W	4.60 W
Efficiency	4.3 %	4.2 %

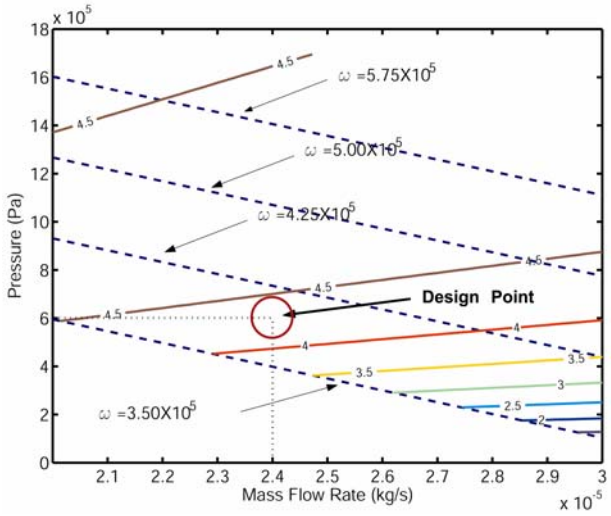

(a) Low Pressure viscous pump

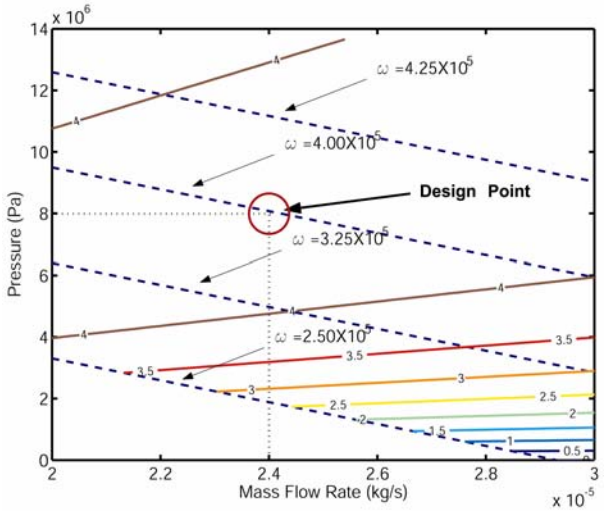

(b) High Pressure viscous pump

Figure 7 - Pump characteristic curves: pressure rise (dashed lines) and efficiency contours (solid lines) as a function of mass flow rate and speed for the low pressure and high pressure designs.

Design optimization was conducted to define the maximum efficiency achievable, while meeting the cycle requirements and matching the rotational speed of the turbine. Over a broad range of pressure ratios (from 0.6 MPa to 8 MPa), optimized configurations were found with a maximum

efficiency of 4-5%. Two configurations are summarized in Table 2 for low pressure and high pressure operation. Figure 7 depicts the pumping curves for both designs, showing the pressure rise curves for different rotational speeds (dashed lines) and predicted efficiency contours (solid lines, labeled in percentages), as a function of mass flow rate. Since these predictions are based on well established analytical formulations that are increasingly valid at low Reynolds numbers, their accuracy is expected to be relatively good compared to the turbine flow field predictions. Inertial effects in the entry region, cavitation, and heat transfer in the pump will however require further assessment.

Heat Exchangers

In the Rankine cycle device considered here, heat needs to be added and removed from the working fluid through heat exchangers, the evaporator and the condenser respectively. They each consist of two main parts: microchannel two-phase flow heat exchangers through which the working fluid travels, and the external heat transfer surface in contact with the heat source or heat sink. The surfaces of the chip are the interface between the internal and external parts of the heat exchangers. In the case where convection is used to provide/remove the heat to/from the chip, the external part of the heat exchanger is limiting, since flow boiling in the internal microchannels provides higher heat transfer rates, hence requiring less area. External heat sink optimization presented elsewhere [22] suggests that it is possible to remove 50-100W of heat per cm^2 by forced air convection with less than 1 W of fan power. In this section, the internal two-phase flow part of the heat exchangers will be considered. Of main interest are the pressure drop and area required to evaporate and fully superheat a constant water stream. Microscale boiling flow is an active research area, mostly focusing on electronic cooling requirements ([23],[24],[25]). Flow phenomena remain poorly understood at this small scale and validated modeling approaches have not yet been developed. Although very high heat transfer rates have been achieved, stable operation in superheated conditions was rarely reported. Typically, dry-out, bubbles, and unsteady flow phenomena prevent stable superheated operation.

To estimate the area required and pressure drop incurred by the heat exchangers, the channel was decomposed in three sections: 1) liquid pre-heating, 2) two-phase flow boiling, and 3) vapor superheating. Traditional internal flow heat transfer and hydrodynamic relations were used in the single-phase flow sections. An optimum configuration of the superheating section (#3) for minimal pressure drop at the design flow rate consisted of 90 parallel channels of 100x50 microns, with a length of less than 0.5 mm. The pressure drop was less than 5 kPa, which induces a negligible load on the pump. The pre-heating section (#1) was comparatively negligible, in pressure drop and length. Although the two-phase flow section remains to be defined, these scales suggest that ample space is available on the $1cm^2$ chip. Furthermore, this suggests that proper distribution of the microchannels will be required in order to provide a uniform heat load over the chip area. Most importantly, further research and development is required in order to define a viable configuration for the phase change section.

Bearings and seals

Two types of bearings are required for the proposed device: thrust bearings for axial support and journal bearings for in-plane support of the rotor. This section first describes the approach for axial balance, followed by a discussion of approaches for in-plane support and sealing. In all cases, a fraction of the core pressurized flow is used to lubricate the bearings. These secondary flows and the forces induced are the main focus.

Axial balance - The main axial forces on the rotor include a pressure force acting downwards on the turbine side, an electromechanical attraction force in the generator (also acting downwards on the rotor), and other pressure forces from the bearings and pump. In order to compensate for a predominately downward force, the bottom side of the disk is used as a thrust balance piston, by drawing a small fraction of high pressure steam from the turbine inlet. The flow extracted from the turbine flow gets into the bottom side through holes or slits on the disk, and comes out of the bearing past a flow restriction, as illustrated by the red flow path in Figure 8. The bearing surface between 3 and 4 consists of a simple circumferential protrusion that is used to control the fractional flow rate and the pressure distribution along the bottom side between point 2 and 3. Pressure gradually drops as the steam flows radially under the disk and then exhibits a sudden drop across the restrictor. Initially, the bearing restrictor is designed to balance out the other forces acting on the rotor, at a design axial position. At the given condition below, the flow rate for the axial balance is >1% of the flow rate through the turbine when the gap g_1 is 1 micron.

This configuration also provides a stabilizing (i.e. restoring) force when the rotor is perturbed from equilibrium. If the rotor is perturbed slightly downward, gap g_1 of the restrictor will decrease leading to less flow under the disk. The radial pressure drop along the generator clearance will hence be decreased, leading to higher pressure force on the back side. This larger upward force will restore the rotor towards its initial equilibrium position.

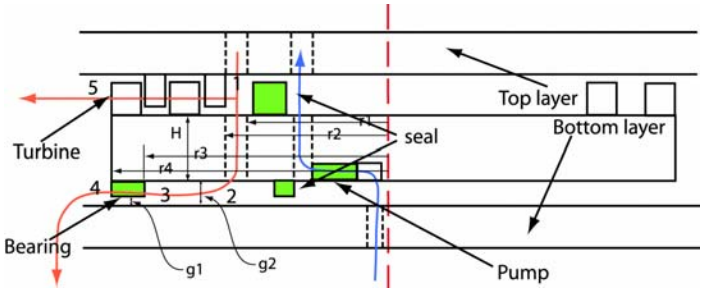

Figure 8 - Cross-section schematic showing the liquid flow path (blue) and steam flow path (red) through the main and secondary flow components. A seal on the back side restricts the high pressure liquid to the inner radius, while the front side seal separates the high pressure steam and liquid. Axial balance is created by bleeding some of the turbine inlet steam under the disk, with the pressure controlled by the outer bearing.

Journal bearing - Two potential locations for the journal bearings are considered: at the inner radius of the disk (center hole) or on its outer radius. The main difference is the state of the lubricating film: steam at the outer radius and liquid at the

inner radius. Micro journal bearing experience to date is limited to gas lubricated bearing at the outer radius of 4 mm diameter rotors with 0.3 mm axial length, which have been demonstrated at high rotational speeds (up to 300 m/s tip speed) [5]. The operating principle consists of driving flow axially along the journal bearing gap, from the backside (4) to the turbine-side of the rotor (5). The axial pressure profile along the sidewall of the rotor is not necessarily linear due to inertial and entry losses, hence it depends on the local gap and Reynolds number. As the rotor moves off-center, the journal bearing gap becomes circumferentially non-uniform, inducing non-uniform pressure forces. Since smaller clearances result in lower inertial and entry losses, local pressure forces are higher that in the large clearance sections, yielding a net re-centering force. In order to minimize the development risks for the Rankine device, a similar configuration is designed herein. From previous experimentation with this type of low aspect ratio hydrostatic journal bearing [5], it was found that journal pressure differentials on the order of 5-30 kPa are required, which are significantly lower than pressures available in the system. Since the turbine exit pressure (location 5) is the lowest in the cycle, slightly pressurized steam will be supplied to the backside (location 4) through internal piping.

Seals - Sealing is required to separate the high pressure fluid from the low pressure fluid and separate the liquid and steam streams. As illustrated in Figure 8, seals are needed at two locations. On the backside of the rotor, a seal must separate the pressurized liquid from entering the backside of the rotor, otherwise, viscous drag in the generator gap would overwhelm other forces on the rotor and drastically impact performance and efficiency. To minimize leakage, an outward flow pump is preferable since the pressure difference across the seal would only be the pressure drop across the evaporator. Two potential seal configurations are considered: a planar annular clearance or a herringbone spiral groove surface. Calculations suggest that the planar clearance with a gap of 1 micron or less would lead to negligible leakage flow rate, and that a patterned seal surface is not necessary. Such clearances are readily implemented and controlled in MEMS. It must be ensured however that the leakage flow evaporates when mixing with the superheated steam that flows over the backside of the disk. Alternatively, an inward flow pump could be considered, such that steam leaks into the pump, however leakage flow rate is significantly higher due to the high pressure difference across the seal.

The top side seal consists of a herringbone spiral groove surface, that also serves as a forward thrust bearing. Its larger radial extend necessary for its bearing functions naturally leads to improved sealing, and is therefore less of a concern than the backside seal.

Generator

The electromagnetic generator design will be directly based on the technology developed at MIT for Watt-scale, microfabricated motors and generators ([16],[26],[27]). Although specific design studies have not been carried out for the Rankine device, such electromechanical technology is expected to be appropriate since the operating conditions and fabrications constraints are similar, and even more conservative, that the gas turbine applications these are currently being developed for. Specifically, magnetic materials are more likely to be applicable given the lower operating temperature in the Rankine cycle compared to the Brayton cycle. Also, the mechanical strength requirements of the rotor components are relaxed since the centrifugal loads are approximately one third that expected in the MIT micro gas turbine, based on design speeds. Based on analysis and experiments to date, power levels on the order of 1-3 W (per rotor) and electromechanical energy conversion efficiency on the order of 50% is expected for such micro-motors and generators. The power density is somewhat lower than required, but future development efforts at MIT are aiming at increase the power output. This and other components efficiencies will be used next to predict system-level performance and efficiency of micro Rankine devices.

PREDICTED SYSTEM PERFORMANCE

The performance of such energy conversion systems can be predicted based on the temperatures of the heat source and heat sink, the component efficiencies, and the mass flow rate. Cycle studies have shown that the Rankine cycle can provide shat power with efficiencies ranging from 15-45%, assuming reasonable turbine and pump efficiencies and practical operating conditions. The net output power will be affected by viscous losses, such as bearing friction, seal drag, and disk windage (viscous drag other than in the bearings and seals), as well as ohmic losses in the generator and power electronics. Figure 9 presents the predicted performance for three different configurations: 1) the top bars are for a high superheated temperature (800°C) and high pressure (8 MPa) device operating in-flight (-50°C ambient); 2) the mid bars are also for in-flight application, but with a lower temperature (400°C) and pressure (0.6 MPa) device, and; 3) the lower bars are this same device, but for ground applications (25°C ambient). This last configuration requires active cooling with a fan that is driven by a fraction of the micro Rankine device output. Water is used as the working fluid.

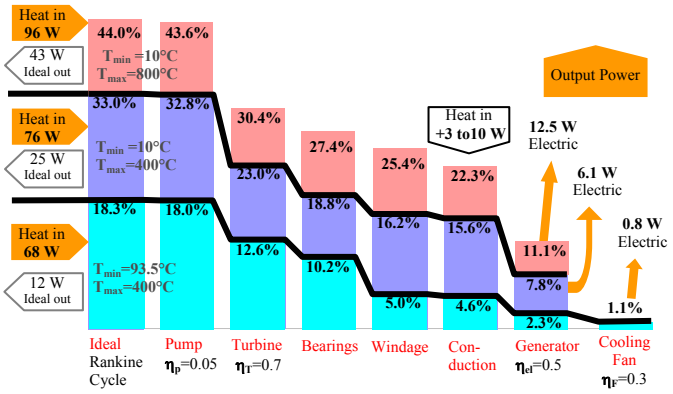

Figure 9 - Predicted performance of the Micro Steam Turbine Power Plant-on-a-chip for three configurations. Bars illustrate the reduction in power as the various sources of loss in the system are incrementally considered, from left to right (water 24mg/s, P_{max}=0.6 MPa).

Depending on the device operation and the application, the output power is predicted to be on the order of 1-12 W for a total heat input of 70-110 W. This corresponds to an energy conversion efficiency of **1-11%** and a power density of **up to 12kW/kg** (assuming a conservative device density of 3g/cm^3).

Such predictions suggests that the proposed technology has comparable efficiency with thermoelectric generators (6.5% for Rankine versus 4.5% for thermoelectrics) for similar operating temperatures (T_{max} = 230°C). The power density is however at least one order of magnitude higher for the micro Rankine device, on par with large scale gas turbine generators. Efficiency and power density can be even higher since the Rankine devices can operate at higher temperatures that allowed for thermoelectric materials. The cost is also expected to be on the order of 1/3 than of thermoelectrics, assuming high volume manufacturing of the Rankine power plants-on-a-chip.

ENGINEERING CHALLENGES

Thermal management

At very small scales, it is difficult to thermally isolate hot structures from cold ones, so preventing heat leakage by conduction becomes critical. For the micro Rankine device, a low thermal resistance between the evaporator and condenser would result in direct conduction heat loss. This heat flux bypasses the cycle, producing no power, and requiring higher heat input (hot side) and removal (cold side). As illustrated in Figure 2, a thin wall of low thermal conductivity material could be used to reduce this heat leakage. Calculations of efficiency as a function of thermal resistance between both sides of the device are shown in Figure 10, and suggest that a silicon connection between both sides of the chip will offer too low of a thermal resistance, but that thin SiO_2 walls would offer sufficient isolation. A *silicon-only* device is therefore not viable due to excessive thermal conduction heat loss. Low conductivity layers between the evaporator and condenser and/or increased separation distance are necessary.

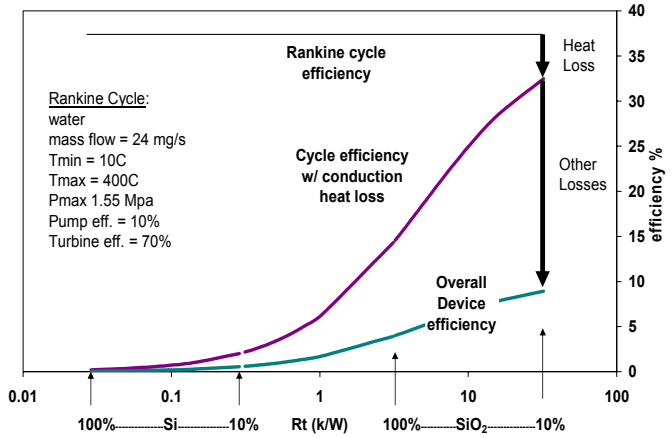

Figure 10 - Impact of structural thermal resistance on efficiency, showing that a silicon junction between the hot and cold sides of the device leads to excessive drop in efficiency, but that small areas of silicon dioxide result in acceptable heat loss (percentages correspond to the ratio of wall area connecting the hot and cold sides to total chip area).

This structure must also provide mechanical functions, such as withstanding the high internal pressures. Generally, higher operating pressures and temperatures increase the cycle efficiency, but may also incur higher conduction heat losses. For example, high pressure operation requires thicker walls to sustain the pressure, which in turn allows greater heat leakage through the structure, and leads to lower efficiency. Thermo-structural considerations were included in the predictions above. Current analysis suggests that higher temperatures are generally beneficial, but that an optimal pressure does exits. Figure 11 illustrates such a trade-off by plotting the cycle efficiency as a function of maximum cycle pressure, with and without thermo-mechanical considerations. With thermal conduction losses, the efficiency shows a maximum value (here around 1.6 MPa), beyond which increased insulating wall thickness is required to sustain the axial pressure load, assuming a maximum allowable bond stress of 1 MPa. Although typical anodic and fusion bond strengths are expected to be higher (above 10 MPa [28]), this suggests that there is an upper limit on practical operating pressures, especially if reasonable safety margins are required. In general terms, thermal isolation in power MEMS is a significant challenge that must be considered when evaluating the viability of a proposed technology.

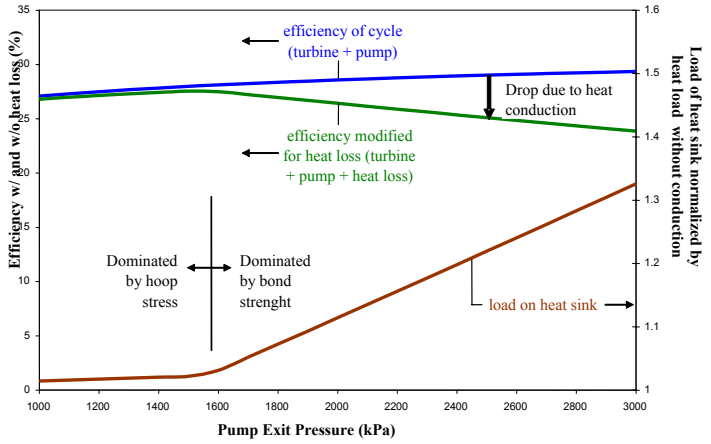

Figure 11 - Impact of thermal conduction heat loss on cycle efficiency as a function of pump exit pressure. Although higher operating pressures improve the cycle efficiency, they require thicker walls to withstand pressure forces, and therefore increase the thermal leakage through the structure.

Efficient microturbomachinery

Low Reynolds number regime in microturbomachinery (ranging from 100 to 10,000) results in higher viscous losses and lower adiabatic efficiency that traditional turbomachinery. Figure 12 illustrates this trend for a turbine vane by plotting the relative total pressure loss coefficient as a function of Reynolds number, calculated using a commercial CFD software (Fluent v6). The sharp increase in loss coefficient below *Re*~100 suggest a minimal practical scale for turbomachinery. Previous numerical investigations of low Reynolds number turbomachinery suggest that efficiency on the order of 70% is expected for millimeter-scale rotors [18]. For the Rankine device, the turbine efficiency is critical since the overall system efficiency scales directly with it. Rotors must be operated at high speeds (100's m/s) and remain at millimeter scale diameters in order to maintain acceptable Reynolds number and limit the impact of viscous losses. From a system-level perspective, the device can be scaled by increasing the design flow rate. This would promote higher velocities and/or larger

rotor diameters (hence potentially higher turbine efficiency), while requiring a larger chip area to accommodate the increased heat load. Scaling of the device will therefore be reconsidered once further knowledge of low Reynolds number turbine aerodynamics is gained, in order to find the appropriate compromise between turbine efficiency and fabrication constraints.

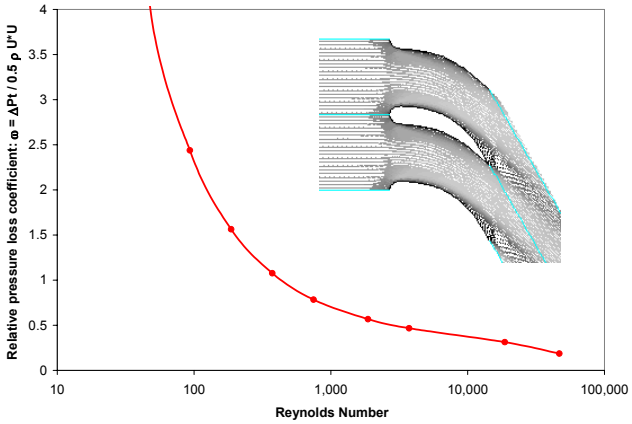

Figure 12 - Relative pressure loss coefficient as a function of scale, represented by the Reynolds number.

High speed microbearings

Although high speed rotation of microfabricated rotors has been demonstrated [13], the ability to design novel MEMS-based configurations based on fundamental understanding remains limited. Further development of validated analytical fluid film microbearing and rotordynamic models will be required. The low aspect ratio characteristic of microfabricated structures departs from traditional bearing configurations, hence the well established knowledge-base does not typically account for some of the most important phenomena encountered, such as hydrostatic stiffness and damping due to axial flow through the journal bearing. The further lack of experience with liquid bearings of this type also impedes short term development efforts and would require further attention. The fluid film bearing approach still holds great promise given its successful implementation at large scale, wide variety of designs (unexplored to date), low wear and acceptable drag.

Microscale two-phase flow

A unique aspect of the Rankine cycle is the presence of liquid and vapor phases. Although this benefits the cycle efficiency by minimizing pumping work, it requires the microscale implementation of evaporators, condensers, and seals. Unfortunately, an engineering basis has not yet been established for the design of such micro-scale components, hence further fundamental and applied work in required. For example, the evaporator must provide a constant flow of superheated steam, without flow pulsations, bubbles, or burn-out regions. In addition, condensation in the turbine may be enhanced by the non-adiabatic nature of microsystems, i.e. large convective heat transfer coefficients and small temperature differences through the structure. Experimental investigations appear as the most amenable approach for addressing these issues and improving the knowledge-base for the design of two-phase flow microsystem components.

Design robustness

Finally, successful development of highly integrated systems, such as the micro Rankine device, requires acceptable operation of the components over a relatively wide range of off-design operating conditions. Manufacturing tolerances, simplified components models, and ill-defined two-phase flow physics are examples of potential sources of variability that can adversely affect a development program. Experimental and numerical work on the key components along with a design approach focused on robustness is therefore important. For example, the aerodynamic design of the multistage turbine should not experience drastic changes of loss and blockage when operating at off-incidences, to ensure acceptable operation if it is mismatched with the other components. Unfortunately, designing for robustness typically implies conservative operating conditions and consequently lower output power levels.

CONCLUSIONS

System-level and component design studies have been carried out for a miniature heat engine implementing the Rankine power cycle using MEMS-based, high performance micromachinery. These suggest that high power density microsystems (up to 12 kW/kg) for power generation appear possible, with efficiency levels on the order of 1-11%, depending on the application. The design space for micromachined multistage turbines and viscous pumps were explored to confirm that viable designs are possible for this application. The viability of other components is also discussed, including the bearing systems, seals, heat exchangers, and generator. Thermal isolation to prevent conduction heat loss was found to be critical, but approaches that limit its impact on system efficiency appear viable. However, many engineering challenges remain before complete Rankine microsystems can be effectively demonstrated.

In order to meet these challenges, current research work is focusing on two key subsystems: 1) the rotating portion of the micro Rankine power plant-on-a-chip, which includes the multistage turbine, pump, bearings, and seals; and 2) the hot section, specifically the evaporator with a focus on robust configurations to provide a stable flow of superheated steam.

If successfully developed, micro Rankine devices could allow lightweight and compact power sources for portable application or high power density energy scavenging from waste heat or solar radiation. The core components would also provide a basis for the future development of micro-refrigeration cycles to cool electronics, sensors, or people, as well as micro hydraulic sources for small robots and vehicles.

ACKNOWLEDGMENTS

Early discussions and contributions of Dr. Norbert Müller, Ying-Ting Yang, and Ajay Rishi are greatly appreciated. This work was supported by the NASA Glenn Research Center, Revolutionary Aeropropulsion and Power Concepts and Technology program (contract NAS3-02118), monitored by Dr. Glenn Beheim. The authors gratefully acknowledge this support.

REFERENCES

[1] Epstein A.H. and Senturia S.D., 1997, "Macro Power from Micro Machinery", Science, **276**, p.1211.

[2] Epstein, A.H., et al. 1997, "Micro-Heat Engines, Gas Turbines, and Rocket Engines - The MIT Microengine Project," AIAA Paper 97-1773, *28th AIAA Fluid Dynamics Conference*, Snowmass Village.

[3] Epstein A.H, Jacobson S.A., Protz J., Fréchette L.G., 2000, "Shirtbutton-Sized Gas Turbines: The Engineering Challenges of Micro High Speed Rotating Machinery," *Proc. 8th Int'l Symp. on Transport Phenomena and Dynamics of Rotating Machinery*, Honolulu, Hawaii.

[4] Isomura, K., Murayama, M., Yamaguchi, H., Ijichi, N., Asakura, H., Saji, N., Shiga,O., Takahashi, K., Tanaka, S., Genda, T., Esashi, M., 2002, "Development of Microturbocharger and Microcombustor for a Three-Dimensional Gas Turbine at Microscale," *ASME IGTI 2002 TURBO EXPO*, Paper GT-2002-30580, Amsterdam, Netherlands, June 6.

[5] Fu, K., Knobloch, A.J. , Martinez, F.C., Walther, D.C., Fernandez-Pello, C., Pisano, A.P. and Liepmann, D., 2001, "Design and Fabrication of a Silicon-Based MEMS Rotary Engine," *Proc. ASME Int'l Mech. Eng. Congress and Expo.*, New York, November 11-16.

[6] Toriyama, T., Hashimoto, K., Sugiyama, S., 2003, "Design of a Resonant Micro Reciprocating Engine for Power Generation," Proc. *Transducers'03*, Boston, MA, June.

[7] Richards, C.D., Bahr, D.F., Xu, C.-G., Richards, R.F., 2001, "The P3 Micro Power Generation System," *Proc. ASME Int'l Mech. Eng. Congress and Expo.*, New York, November 11-16.

[8] Santavicca, D., Sharp, K., Hemmer, J., Mayrides, B., Taylor, D., Weiss, J., 2003, "A Solid Piston Micro-engine for Portable Power Generation," *Proc. ASME Int'l Mech. Eng. Congress and Expo.*, Washington, D.C., Nov. 16-21.

[9] Schaevitz, S.B., Franz, A. J., Jensen, K. F. and Schmidt, M. A., 2001, "A Combustion-based MEMS Thermoelectric Power Generator," Proc. *Transducers'01*, Munich, Germany, June 10-14, pp. 30-33.

[10] Sitzki, K. Borer, S. Wussow, E. Schuster, P.D. Ronney and Cohen, A., 2001, "Combustion in Microscale Heat Recirculating Burners," *39th AIAA Aerospace Sciences Meeting*, Paper No. 2001-1087, Reno, NV, January 8-11.

[11] Zhang, C., Najafi, K., Bernal, L.P., Washabaugh, P.D., 2003, "Micro Combustion-Thermionic Power Generation: Feasibility, Design and Initial Results". *Proc. Transducers'03*, Boston, MA, June.

[12] Nielsen, O.M., Arana, L.R., Baertsch, C.D., Jensen, K.F., Schmidt, M.A., 2003, "A Thermophotovoltaic Micro-Generator for Portable Power Applications," *Proc. Transducers'03*, Boston, MA, June.

[13] Fréchette, L.G., Jacobson, S.A., Ehrich, F.F., Ghodssi, R., Khanna, R., Wong, C.W., Zhang, X., Schmidt, M.A., Epstein, A.H., 2000, "Demonstration of a Microfabricated High-Speed Turbine Supported on Gas Bearings," Tech. Digest, *Solid-State Sensor and Actuator Workshop*, Hilton Head Is., SC, pp. 43-47.

[14] Mehra, A., Zhang, X., Ayón, A. A., Waitz, I. A., Schmidt, M. A., Spadaccini, C., 2000, "A Six-Wafer Combustion System for a Silicon Micro Gas Turbine Engine," *J. Microelectromechanical Systems*, vol. 9, no. 4, pp. 517-527.

[15] London, A.P., Epstein, A. H., Kerrebrock, J. L., 2001, "High-Pressure Bipropellant Microrocket Engine," *AIAA J. Propulsion and Power*, vol. 17, no. 4, pp. 780-787.

[16] Fréchette, L.G., Nagle, S.N., Ghodssi, R., Umans, S.D., Schmidt, M.A., Lang, J.H., 2001, "An Electrostatic Induction Micromotor Supported on Gas-Lubricated Bearings," *Proc. 14th IEEE Int'l Conf. on Micro Electro Mechanical Systems*, Interlaken Switzerland, Jan 21-25, pp. 290-293.

[17] Kerrebrock, J.L., 1992, *Aircraft engine and gas turbines*, 2nd Ed., MIT Press, Cambridge, MA.

[18] Mehra, A., 1997, *Computational Investigation and Design of Low Reynolds Number Micro-Turbomachinery*. S.M. Thesis, Massachusetts Institute of Technology, Cambridge, MA.

[19] Muijderman, E. A., 1966, *Spiral Groove Bearings*, Springer-Verlag New York.

[20] Sato, Y., Ono, K., and Iwama, I., 1990, "The Optimum Groove Geometry for Spiral Groove Viscous Pumps," *ASME J. Lubrication Tech.*, vol. 112, no. 2, pp. 409-414.

[21] Hsing, F. C., 1974, "Analytical Solutions for Incompressible Spiral Groove Viscous Pumps," *ASME J. Lubrication Tech.*, vol. 96, no. 3, pp. 365-369.

[22] Meuller, N., Fréchette, L.G., 2002, "Optimization and Design Guidelines for High Flux Micro-Channel Heat Sinks for Liquid And Gaseous Single-Phase Flow," *Proc. 8th Intersociety Conf. on Thermal and Thermomech. Phenomena in Elec. Systems* (ITherm2002), San Diego, June.

[23] Mudawar I., 2001, "Assessment of high-heat-flux thermal management schemes," *IEEE Trans. on Components and Packaging Tech.*, vol. 24, no. 2, June, pp. 122 -141.

[24] Koo J. M., et al., 2001, "Modeling of two-phase microchannel heat sinks for VLSI chips," *Proc. 14th IEEE Int'l Conf. on Micro Electro Mechanical Systems*, Interlaken Switzerland, Jan 21-25, pp. 422-426.

[25] Zhang L., et al., 2001, "Study of boiling regimes and transient signal measurements in microchannels," *11th International Conference on Solid-State Sensors and Actuators*, Munich, Germany, June 10-14.

[26] Nagle, S.F., 2000, Analysis, *Design, and Fabrication of an Electric Induction Micromotor for a Micro Gas-Turbine Generator*. Ph.D. Thesis, Massachusetts Institute of Technology, October.

[27] Koser, H., Cros, F., Allen, M.G., Lang, J.H., 2001, "A High Torque Density Magnetic Induction Machine," *Proc. 11th International Conf. on Solid-State Sensors and Actuators (Transducers)*, Munich, Germany, June, pp. 284-287.

[28] Cheng, Y. T., Lin, L., Najafi, K., 2000, "Localized Silicon Fusion and Eutectic Bonding for MEMS Fabrication and Packaging," *J. Microelectromech. Systems*, vol. 9, no. 1.